Mass Accommodation Coefficient of H_2SO_4 Vapor on Aqueous Sulfuric Acid Surfaces and Gaseous Diffusion Coefficient of H_2SO_4 in N_2/H_2O

Ulrich Pöschl,[‡,§] Manjula Canagaratna,[‡] John T. Jayne,[†] Luisa T. Molina,[‡] Douglas R. Worsnop,[†] Charles E. Kolb,[†] and Mario J. Molina*[,‡]

Department of Chemistry and Department of Earth, Atmospheric and Planetary Sciences, Massachusetts Institute of Technology, Cambridge, Massachusetts 02139−4307, and Center for Aerosol and Cloud Chemistry, Aerodyne Research, Inc., Billerica, Massachusetts 01821−3976

Received: June 30, 1998; In Final Form: September 16, 1998

The experimental determination of the mass accommodation coefficient of H_2SO_4 vapor on aqueous sulfuric acid and the gas-phase diffusion coefficient of H_2SO_4 vapor in N_2/H_2O at 303 K is reported. The measurements were carried out under laminar flow conditions in a coated wall tubular flow reactor coupled to a chemical ionization mass spectrometer for gas-phase detection. Wall loss rates of H_2SO_4 vapor, from which both the mass accommodation coefficient and the gas diffusion coefficient were determined, were measured as a function of total reactor pressure, water vapor concentration, and sulfuric acid vapor concentration. The observed wall loss rate coefficient depends linearly on the inverse of the total reactor pressure (0.54−10 Torr) and is independent of the aqueous sulfuric acid composition over the range 73−98 wt %, which was varied by the addition of water vapor. A kinetic model based on the additivity of kinetic resistances that couples gas-phase diffusion and mass accommodation to the measured H_2SO_4 vapor loss rate has been applied to the data. The model yields a lower limit of 0.43 with a best fit value of 0.65. The mass accommodation coefficient is independent of the liquid H_2SO_4/H_2O composition over the range investigated. The gas-phase diffusion coefficient for H_2SO_4 vapor in N_2/H_2O (H_2O mixing ratio ≤ 0.32) was determined to be 66.8 ± 1.1 Torr cm^2 s^{-1}. The resistance model agrees well with a more rigorous approximate solution to the full continuity equation describing mass transport and kinetics. The atmospheric implications of the reported results are discussed.

Introduction

Sulfate aerosols are formed in both the earth's troposphere and stratosphere where they backscatter incident sunlight, resulting in significant radiative forcing that directly influences climate.[1,2] Furthermore, sulfate aerosols are known to play a key role in nucleating and stabilizing tropospheric clouds, which scatter incident sunlight as well as intercept outgoing infrared radiation, resulting in a significant indirect effect on radiative forcing.[1,3] Finally, sulfate aerosols play a critical role in the chemistry of stratospheric ozone depletion, both by directly catalyzing the heterogeneous conversion of reservoir compounds such as N_2O_5, $ClONO_2$, and $BrONO_2$ to sequester reactive nitrogen oxides and, in the case of halogen nitrates, release more photochemically active halogen and hydrogen oxide radical precursors and by nucleating the formation of larger polar stratospheric cloud particles which also catalyze key heterogeneous processes leading to dramatic springtime ozone loss in polar regions.[4,5]

Atmospheric sulfate aerosols are formed from gaseous sulfur dioxide, SO_2, which is either emitted directly into the atmosphere or formed in situ by oxidation of gaseous reduced sulfur compounds primarily emitted by biogenic sources.[5−7] SO_2 can be oxidized to sulfuric acid, H_2SO_4, by reacting either heterogeneously on/in aqueous aerosols or cloud droplets with H_2O_2, O_3, or O_2 or homogeneously with OH, O_2, and H_2O vapor.[5−8] Gaseous H_2SO_4 formed in this latter process (via the Calvert and Stockwell mechanism,[9] modified by a second-order reaction of SO_3 with H_2O vapor[10]) can have two fates. The first, heterogeneous scavenging by preexisting aerosol or cloud droplets, generally leads to larger aerosol particles (most cloud droplets evaporate producing aerosol particles) but no additional particles. The second, homogeneous nucleation of H_2SO_4 and H_2O vapors[5−8] (with the possible involvement of NH_3 and/or volatile organics[11]), is believed to be responsible for the formation of new particles (secondary aerosol) in the ambient troposphere and stratosphere, as well as in the plumes of aircraft exhausting sulfur oxides into the atmosphere.[12]

Whether or not H_2SO_4 vapor will stick to preexisting aerosol or build up to concentrations capable of nucleating new particles depends strongly on the magnitude of its mass accommodation coefficient, α, on various aerosol surfaces.[5,6,12] The mass accommodation coefficient for H_2SO_4 vapor has been subject to considerable uncertainty. Van Dingenen and Raes reported a low value of $0.02 < \alpha < 0.09$ on aqueous H_2SO_4 deduced from measuring the rate of particle growth in a batch reactor.[13] Similarly, small theoretical values for the H_2SO_4 "sticking" coefficient on aqueous surfaces based on a unimolecular transition-state treatment were reported by Itoh.[14] However, this theoretical analysis was discounted by Clement et al., who used a simple classical two-body model to predict "sticking" coefficients near unity for this system.[15] Note that neither of these theoretical studies carefully distinguish between thermal or momentum accommodation, meaning that the surface stops the vapor molecule, and mass accommodation, meaning that

* To whom correspondence should be addressed.
‡ Massachusetts Institute of Technology.
† Aerodyne Research, Inc.
§ Current address: Max-Plank Institute for Chemistry, Atmospheric Chemistry Division, Becherweg 27, D-55128 Mainz, Germany.

10.1021/jp982809s CCC: $15.00
Published on Web 11/11/1998

the vapor molecule penetrates the gas−liquid interface and enters the liquid phase.[16] Quite recently, Jefferson et al. used an aerosol flow reactor with chemical ionization mass spectrometric detection to directly measure large values of α at room temperature on $(NH_4)_2SO_4$ ($\alpha = 0.73 \pm 0.21$) and NaCl ($\alpha = 0.79 \pm 0.23$) aerosols.[17] Also, De Bruyn et al. used a droplet flow reactor technique to directly measure $\alpha = 0.12$ for the related species methanesulfonic acid (MSA) on water surfaces at 273 K; they found a strong negative temperature dependence between 280 and 260 K, with α reaching 0.18 at 260 K.[18]

In this paper we report the first direct measurements of the mass accommodation coefficient of sulfuric acid vapor on liquid H_2SO_4/H_2O surfaces, a parameter required to accurately model aerosol microphysics of the ambient atmosphere as well as aircraft exhaust plumes.[5,6,12] We also report measurements of the gaseous diffusion coefficient for H_2SO_4 vapor in N_2/H_2O mixtures. Our results were obtained with a wetted wall flow reactor apparatus equipped with chemical ionization mass spectrometer detection.

Experimental Section

The kinetic experiments were performed in a fast flow reactor coupled to a chemical ionization mass spectrometer and operated under low-pressure laminar flow conditions. The apparatus has been described in detail previously.[10] The flow reactor is a cylindrical Pyrex glass tube, 2.2 cm i.d. and 100 cm in length. Dry N_2 from a liquid nitrogen gas pack (BOC Gases) was used as the carrier gas. All carrier flows were monitored with calibrated electronic mass flow meters (Tylan General, Matheson Gas Products). The flow reactor was connected to a 1600 L min^{-1} rotary pump (Edwards EM280) equipped with a throttle valve; the reactor pressure was monitored by a 0−10 Torr pressure gauge (MKS Baratron). Temperatures were measured by calibrated copper−constantan thermocouples (Omega Engineering). All electronic signals were monitored and processed via a PC-based data acquisition system.

H_2SO_4 vapor was introduced into the flow reactor through a central moveable injector. The tip of this injector is equipped with a small glass container filled with glass wool and a sample of liquid sulfuric acid. The temperature of this H_2SO_4 reservoir was controlled by resistive heating, using a PID temperature controller (Omega Engineering, CN-76122) and a thermocouple sealed in a glass capillary and placed inside the reservoir. It was adjusted between 328 and 368 K and stabilized within ±0.1 K. A N_2 carrier gas flow passing through the injector (100−300 sccm) was used to entrain H_2SO_4 vapor from the acid reservoir. Saturation of the carrier gas flow with H_2SO_4 vapor was experimentally verified as described below. The H_2SO_4 reservoir was regularly refilled with ∼0.5 mL of 96.0 wt % H_2SO_4 (Mallinckrodt AR). During the kinetic experiments, the liquid H_2SO_4 sample was continuously kept at low pressure under the N_2 carrier flow. Considering evaporation only, the sample would approach the composition at which the equilibrium partial pressure ratio of H_2SO_4 and H_2O corresponds to the ratio of mole fractions in the liquid phase, i.e., the composition of the azeotropic mixture with a boiling point equal to the sample temperature. For the usual injector temperatures between 328 and 368 K this would imply H_2SO_4 concentrations above 99 wt %.[19] On the other hand, the N_2 carrier gas flow is not absolutely dry—due to leaks in the vacuum and gas supply system a small amount of air including water vapor (determined from a relative humidity measurement in the room) is entrained into the carrier gas flows. Based on the reactor's leak rate, the H_2O background concentration in the N_2 carrier gas flow is estimated to be $\sim 5 \times 10^{12}$ cm^{-3}; in the injector temperature range from 328 to 348 K this leads to an average sample composition of 98 ± 0.5 wt % H_2SO_4.[19,20] The composition of the H_2SO_4 sample was independent of the water partial pressure in the reactor, since back-diffusion of H_2O into the injector can be neglected under the experimental fast flow conditions. In our experiments the wall coating reached its equilibrium composition within a few minutes, indicated by the quick stabilization of the H_2SO_4 background signal which was determined by the temperature and concentration of the wall coating. Typically 5−10 min was allowed for equilibration between runs with different H_2O concentrations; the signal, however, stabilized much faster, within a couple of minutes. The sulfuric acid coating was a colorless submillimeter layer on the walls with a surface area A given by the cylindrical flow tube geometry: $A = \pi r^2 z$, where r is the flow tube radius and z is the reaction length.

Water vapor was introduced at the upstream end of the of the reactor by controlling a flow of N_2 carrier gas (0−500 sccm) through a water bubbler immersed in a temperature stabilizing bath. After leaving the bubbler through a throttle valve, the water carrier flow was mixed with an additional N_2 gas flow (0−1000 sccm). The temperature inside the bubbler was continuously monitored by a thermocouple immersed in the liquid water sample. Based on the leak rate, the water vapor concentration in the flow reactor was estimated to be $\sim 5 \times 10^{12}$ cm^{-3} when the H_2O source was shut off; with a carrier flow through the bubbler it was controlled in the range from 5×10^{13} to 3×10^{16} molecules cm^{-3}. $[H_2O]$ was calculated from the measured liquid water temperature, the gas flow rates, the reactor pressure, and the bubbler pressure, which was adjusted by the throttle valve between 100 and 760 Torr; the $[H_2O]$ calculation has been described and experimentally verified in a previous study using the same reactor and water source.[10]

H_2SO_4 was detected by chemical ionization mass spectrometry with SF_6^- reagent ions at the downstream end of the flow reactor. The SF_6^- ions were generated by passing neutral SF_6 (∼0.05 sccm, Matheson) in a flow of N_2 (∼1 slpm) through a radioactive polonium ion source (^{210}Po, NRD Nuclecel P-2031). The ion flow from the polonium source was injected through a knee-shaped $^1/_4$ in. o.d. stainless steel tube radially centered in the reactor 6 cm upstream of the mass spectrometer's sampling orifice, allowing ion−molecule reaction times of a few milliseconds. SF_6^- and the product ions were detected with a quadrupole mass spectrometer (Extrel C50) operated in negative ion counting mode and housed in a two-stage differentially pumped vacuum system; the mass spectrometer setup has been described in detail previously. The ions were sampled through a 600 μm orifice held at −120 V. To optimize the measured ion intensities and to control ion clustering by collisional dissociation, a variable voltage was applied to the ion injection tube (−150 to −600 V, depending on the pressure and flow conditions in the reactor). During the kinetic measurements the ratio of the SF_6^- reagent ion intensity to the H_2SO_4 product ion intensities was usually kept above 10 to assure linear detection characteristics,[21] and the product ion signals were normalized with respect to the SF_6^- signal intensity.

The primary ion−molecule reaction between H_2SO_4 and SF_6^- is a proton abstraction which leads to the formation of HSO_4^- ($m/e = 97$) and occurs at a rate near the collision limit.[22] Additionally, we observed the formation of cluster ions, predominantly $[HSO_4 \cdot H_2O]^-$ ($m/e = 115$) and $[HSO_4 \cdot HF]^-$ ($m/e = 117$). As expected, the cluster ion signal intensities increased strongly with increasing reactant concentrations and ion−

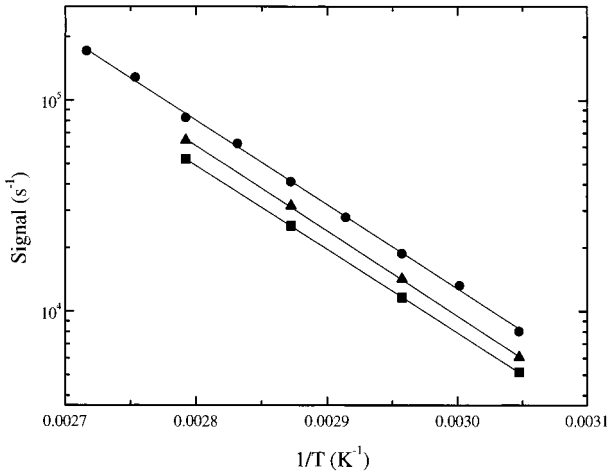

Figure 1. Observed dependence of HSO_4^- (●), $[HSO_4 \cdot HF]^-$ (▲), and $[HSO_4 \cdot H_2O]^-$ (■) ion signals on the temperature of the sulfuric acid vapor source.

molecule reaction times. At high pressures, low flow velocities, and high H_2SO_4 concentrations we could also observe $[HSO_4 \cdot (H_2SO_4)_n]^-$ clusters with n up to 6, but under the conditions we usually maintained during the kinetic experiments only $[HSO_4 \cdot H_2SO_4]^-$ was detectable. During the wall loss experiments the extent of ion clustering was controlled by adjustment of the voltages applied to the ion-injection tube and the sampling orifice plate. Enhancement of the potential difference and the electric field in the ion−molecule region lead to enhanced collisional dissociation; at high potential differences (ca. ∼100 V at 2 Torr and ∼400 V at 4 Torr) practically all H_2SO_4 cluster ions could be collisionally dissociated and detected as HSO_4^-. The potential difference needed for complete dissociation of $[HSO_4 \cdot H_2O]^-$ and $[HSO_4 \cdot HF]^-$ was about 10% lower than for $[HSO_4 \cdot H_2SO_4]^-$, which indicates that the latter complex is more strongly bound. Generally, we used the HSO_4^- ion signal to monitor the H_2SO_4 concentration in our kinetic experiments. Alternative measurements using the $[HSO_4 \cdot H_2O]^-$ and $[HSO_4 \cdot HF]^-$ signals were in excellent agreement with the measurements based on the HSO_4^- signal (less than 5% scatter of the observed decay rates). The H_2SO_4 detection sensitivity at a signal/noise ratio of 1 was $\sim 10^{10}$ cm^{-3}.

Linear detection of H_2SO_4 over the concentration ranges used in our experiments was verified by monitoring the HSO_4^-, $[HSO_4 \cdot H_2O]^-$, and $[HSO_4 \cdot HF]^-$ signals as a function of N_2 carrier flow through the injector and injector temperature under otherwise unchanged conditions (fixed injector position, constant total flow and pressure, constant $[H_2O]$). In a series of test experiments the observed ion signals showed a linear proportionality with the carrier gas flow and exhibited the expected logarithmic dependence on the inverse of temperature. In Figure 1 the signals for HSO_4^- (circles), $[HSO_4 \cdot HF]^-$ (triangles), and $[HSO_4 \cdot H_2O]^-$ (diamonds) in Hz are plotted versus the inverse of temperature; the measurements were performed at 2 Torr total pressure and three different water partial pressures in the reactor. Following the formalism applied by Ayers et al.,[23] the observed temperature dependence, i.e., the slope of linear fits like the ones shown in Figure 1, can be expressed in terms of the vaporization enthalpy of pure sulfuric acid and the chemical potential difference for H_2SO_4 in pure sulfuric acid and in the observed aqueous sample. Using the chemical potential for H_2SO_4 in 98 wt % sulfuric acid as tabulated by Giauque et al.,[24] an average value of 78 ± 7 kJ mol^{-1} (95% confidence level) is obtained for the vaporization enthalpy of pure sulfuric acid. This value is in reasonable agreement with the value of 84.4 kJ mol^{-1} determined by Ayers et al.[23] and the value of 79.1 kJ mol^{-1} calculated by Gmitro and Vermeulen.[25] These results indicate that the injector gas flow is indeed saturated with H_2SO_4 and confirm that the back-diffusion of H_2O into the injector is negligible. They also clearly demonstrate that all three ion signals, HSO_4^-, $[HF \cdot HSO_4]^-$, and $[H_2O \cdot HSO_4]^-$, are directly proportional to the H_2SO_4 concentration at the exit end of the flow reactor. Based on the geometry of the ion−molecule reaction region, the flow conditions, and the orientation of the sampling orifice, the ion signals are assumed to be proportional to the radially averaged H_2SO_4 concentration.

During the kinetic measurements the H_2SO_4 reservoir in the injector tip was kept at a constant temperature between 328 and 348 K. After entering the flow tube reactor the injector gas flow, which is saturated with H_2SO_4 vapor in equilibrium with the hot liquid H_2SO_4 sample, is rapidly thermalized to the reactor temperature which was 303 ± 2 K throughout the kinetic experiments. About 2 cm downstream of the injector tip (corresponding to ∼1 to 4 ms flow time) the gas temperature was generally less than 5 K above the average reactor temperature. Consequently, the gas phase downstream of the reactor is supersaturated with H_2SO_4 vapor which leads to the deposition of H_2SO_4 on the reactor walls and to the formation and growth of an aqueous sulfuric acid wall coating. The composition of the sulfuric acid wall coating is determined by the partial pressure of H_2O which will be discussed below. Initial H_2SO_4 gas-phase concentrations (radial average at the injector tip) were estimated using the vapor pressure equation given by Ayers et al.[23] under the assumption of an average sample concentration of 98 wt % H_2SO_4.

The experiments were performed under laminar flow conditions with Reynolds numbers ranging from 10 to 100 at total reactor pressures, P, from 0.54 to 10.0 Torr. The average flow velocities, v, ranged from 400 to 2500 cm s^{-1} and were calculated by

$$v = (F_t + F_w)\frac{760}{P}\frac{T}{273}\frac{1}{r^2\pi} \qquad (1)$$

F_t is the sum of all N_2 carrier gas flows (STP cm^3 min^{-1}) measured by the electronic mass flow meters, and F_w is the flow of H_2O from the bubbler into the reactor, given by $F_w = F_b P_b/(P_b - P_w)$. F_b stands for the N_2 carrier gas flow through the bubbler, P_b is the total bubbler pressure, P_w is the equilibrium water vapor pressure at bubbler temperature, and r is the flow tube radius (centimeters). Under the usual experimental conditions, the entrance length (development of the parabolic velocity profile) and the mixing distance were estimated to be 1.2−12 cm and 4−18 cm, respectively.[26−29] Generally, the mixing distance determined the minimum reaction distance for the kinetic measurements; the reaction distance at which the H_2SO_4 signal started to deviate significantly from the observed first-order decay was mostly ∼30% smaller than the estimated value.

Results

The condensation of supersaturated H_2SO_4 vapor, i.e., its net uptake by the sulfuric acid wall coating, can be observed as wall loss process following the simple first-order rate equation

$$\frac{d[H_2SO_4]_{ex}}{dt} = k_{obs}[H_2SO_4]_{ex} \qquad (2)$$

where k_{obs} (s^{-1}) is the first-order rate coefficient. $[H_2SO_4]_{ex}$ is the H_2SO_4 concentration exceeding the saturation level and is defined as $[H_2SO_4]_{ex} = [H_2SO_4]_{tot} - [H_2SO_4]_{eq}$, where $[H_2SO_4]_{tot}$

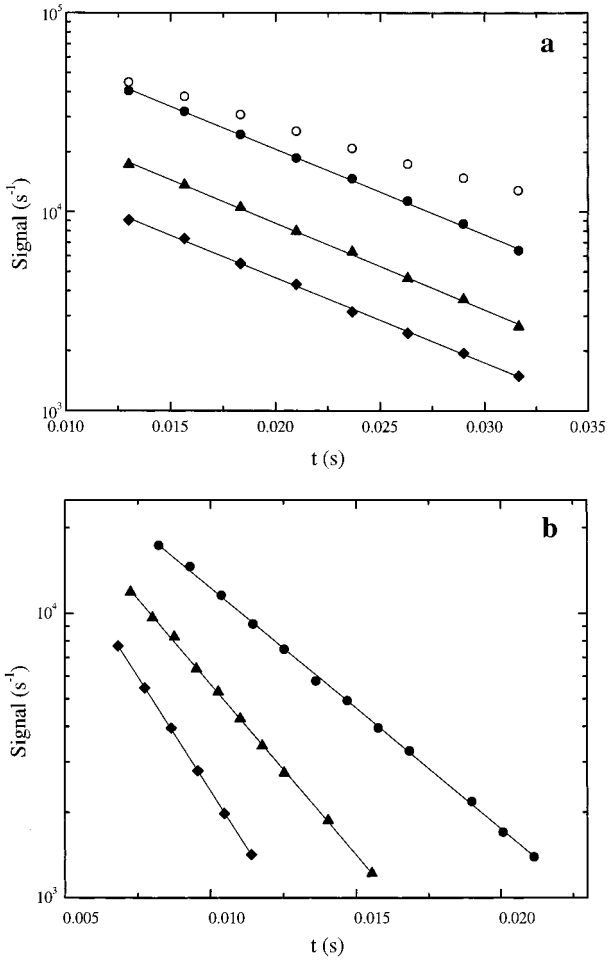

Figure 2. (a) Representative kinetic plot of ion signal versus reaction time. The open circles are HSO_4^- signal without background correction (see text for details). The background corrected signals are HSO_4^- (●), $[HSO_4 \cdot HF]^-$ (▲), and $[HSO_4 \cdot H_2O]^-$ (◆). (b) Observed HSO_4^- signal as a function of reaction time at total pressures of 1 (●), 0.71 (▲), and 0.54 Torr (◆).

stands for the total gas-phase concentration of H_2SO_4 and $[H_2SO_4]_{eq}$ stands for the H_2SO_4 equilibrium concentration corresponding to the vapor pressure of the sulfuric acid wall coating at the reactor temperature.

Experimental runs were carried out by recording the H_2SO_4 ion signal as a function of reaction distance, z (centimeters), between the H_2SO_4 injector and the ion sampling orifice. Reaction distance is converted to reaction time, t (seconds), assuming plug flow conditions: $t = z/v$, where v is the average flow velocity (cm s^{-1}). During each run the water concentration, the injector temperature and the flow conditions were kept constant. Before and after each run the H_2SO_4 background signal, which is proportional to $[H_2SO_4]_{eq}$ and does not vary with injector position, was determined by turning off the carrier flow through the injector. This background signal was subtracted from the total H_2SO_4 signal measured at different injector positions. The resulting background-corrected signal corresponds to $[H_2SO_4]_{ex}$ and was used to determine k_{obs}. For each experimental run a first-order rate coefficient was obtained from the slope of a linear least-squares fit like the ones shown in Figure 2. A typical data set measured at 2 Torr total pressure and $[H_2O] = 3.2 \times 10^{14}$ cm^{-3} is displayed in Figure 2a; the three H_2SO_4 ion signals observed in this experimental run are plotted versus reaction time. The full circles, triangles, and diamonds represent the background-corrected HSO_4^-, $[HSO_4 \cdot HF]^-$, and $[HSO_4 \cdot H_2O]^-$ signals, respectively, which are

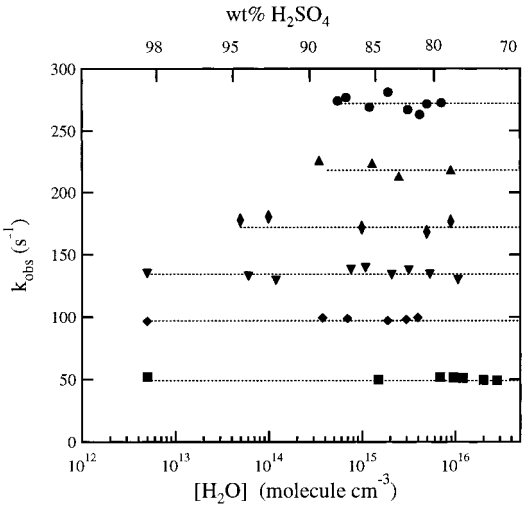

Figure 3. Dependence of the observed wall loss rate coefficients on gas-phase H_2O concentration (lower axis) and composition of the sulfuric acid on the walls (upper axis). The various symbols represent data taken at different total pressures: 0.71 (●), 0.90 (▲), 1.15 (♦), 1.45 (▼), 2.00 (◆), and 4.00 Torr (■). The dashed lines are to guide the eye.

proportional to $[H_2SO_4]_{ex}$. The open circles in Figure 2a are the HSO_4^- raw data without background correction; they are proportional to the total H_2SO_4 gas-phase concentration. The first-order rate coefficients determined from each of the three ion signals shown in the figure are the same within experimental error, varying in the range from 98.2 to 100.4 s^{-1}. Figure 2b shows three data sets measured at 0.54, 0.71, and 1.0 Torr with water vapor concentrations of 7.6×10^{14}, 1.8×10^{15}, and 1.4×10^{15} cm^{-3}, respectively. The linear fits have a common intercept at a signal intensity of 8×10^4 s^{-1}. As discussed below, the different slopes are due to a dependence on total pressure rather than on water vapor concentration.

More than 100 experimental runs were carried out to determine first-order rate coefficients from linear fits such as those shown in Figure 2 to characterize H_2SO_4 wall loss, i.e., condensation rates of supersaturated H_2SO_4 vapor. Measurements were performed over the total pressure range from 0.54 to 10.0 Torr, with initial H_2SO_4 gas-phase concentrations between 2×10^{12} and 4×10^{13} cm^{-3} and with H_2O gas-phase concentrations between 5×10^{12} and 3×10^{16} cm^{-3}. The observed rate coefficients show no significant dependence on the partial pressures of H_2SO_4 and H_2O and thus no dependence on the composition of the sulfuric acid wall coating, which will be discussed below. This also implies that any potential homogeneous nucleation and subsequent mass accommodation on H_2SO_4/H_2O particles did not influence our results. Figure 3 shows the k_{obs} values obtained from individual experimental runs at six different pressures and various H_2O concentrations. The rate coefficients do, however, exhibit a linear dependence on the inverse of total pressure, indicating that the wall loss is diffusion limited. This is shown in Figure 4 where the rate coefficient k_{obs} is plotted versus $1/P$; the data points represent averages of 2−8 measurements with standard deviations of 2−6%; the error bars are 2σ. The overall accuracy in the experimental determination of k_{obs} is estimated to be better than ±20%. The data points shown in Figure 4 are also given in Table 1 and were used to determine the gas-phase diffusion coefficient and the mass accommodation coefficient, as discussed below.

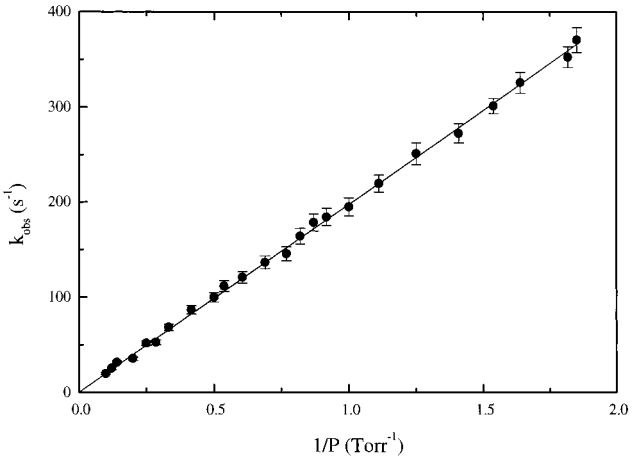

Figure 4. Observed rate coefficient plotted as a function of the inverse of the total pressure. Each point on the plot is an average of 2−8 measurements performed at the same total flow tube pressure (data from Table 1). The error bars on each data point represent the experimentally observed scatter ($\pm 1\sigma$). The solid line is a linear least-squares fit to the data (see "diffusion" subsection of discussion for details).

TABLE 1: Pressure Dependence of the Observed Wall Loss Rate Coefficients

P (Torr)[a]	k_{obs} (s^{-1})[b]	error (s^{-1})[c]	P (Torr)[a]	k_{obs} (s^{-1})[b]	error (s^{-1})[c]
0.54	370.44	13.00	1.45	136.50	6.83
0.55	352.50	11.00	1.65	120.75	6.04
0.61	325.71	11.00	1.86	111.56	5.58
0.65	301.20	8.00	2.00	99.75	4.99
0.71	272.40	10.00	2.40	86.63	4.33
0.80	250.95	11.55	3.00	68.25	3.41
0.90	219.60	9.00	3.50	52.50	2.63
1.00	195.05	9.50	4.00	51.45	2.57
1.07	184.28	9.21	4.97	35.44	1.77
1.15	178.50	8.93	7.11	31.50	1.58
1.22	164.06	8.20	8.20	25.20	1.26
1.30	145.69	7.28	9.97	19.69	0.98

[a] Total pressure in the flow tube. [b] Average wall loss rate coefficient obtained from 2 to 8 kinetic runs at the given flow tube pressure. [c] Observed 1σ scatter in the rate coefficients of the averaged runs.

Discussion

Wall Loss Rate Coefficient. In our flow tube experiments, some sulfuric acid molecules are incorporated into the liquid surface, while others evaporate from the liquid. As discussed above, eq 2 relates the rate constant k_{obs}, which characterizes the measured decays, to $[H_2SO_4]_{ex}$, which is the difference between the actual gas-phase concentration of sulfuric acid and its equilibrium concentration. Clearly, $[H_2SO_4]_{ex}$ behaves in the same manner as the concentration of a gas that condenses at the flow tube walls but does not evaporate from the walls. Thus, the net flux of H_2SO_4 into the condensed phase, J_n, can be assumed to be proportional to the excess gas-phase concentration at the wall, $([H_2SO_4]_{ex})_w$:

$$J_n = \kappa_w([H_2SO_4]_{ex})_w \tag{3}$$

The proportionality constant κ_w is a wall loss rate coefficient in units of cm s^{-1}, equivalent to a deposition velocity.

Using (3) as a boundary condition, the continuity equation for $[H_2SO_4]_{ex}$ in our steady-state reactor can be solved and κ_w can be related to k_{obs}. Considering diffusion and wall loss in a tubular reactor with laminar flow, the continuity equation has been solved by several groups,[30−32] using various approximations such as neglecting higher order terms in the series expansion that represents the solution. For example, Brown[32] lists a computer program that can be used to calculate a κ_w value for a given value of k_{obs}, D_g (the gas-phase diffusion coefficient), r (the flow tube radius), and v (the average flow velocity).

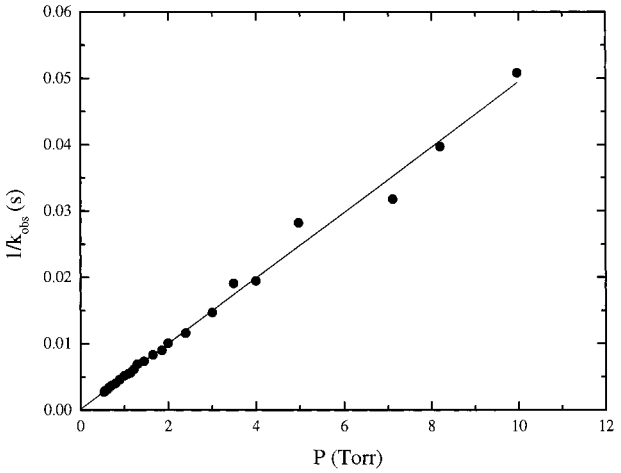

Figure 5. Inverse of the observed rate coefficient plotted as a function of the total flow tube pressure (data from Table 1). The solid line is a weighted linear least-squares fit to the data (see "wall loss rate coefficient" subsection of discussion for details).

An alternative but much simpler approach which is used here and has been suggested by Gershenzon[33] to solve the continuity equation in question involves using the rule of additivity of kinetic resistances:

$$\frac{1}{k_{obs}} = \frac{1}{k_d} + \frac{1}{k_w} \tag{4}$$

Here, $1/k_d$ is the diffusive resistance and $1/k_w$ is the surface uptake resistance. The rule of additivity of kinetic resistances has been successfully applied to other kinetic processes.[34] It is valid if the wall loss is first order in reactant concentration and the diffusive flow to the walls is linearly proportional to the reactant concentration averaged over the cross section of the flow tube minus the concentration at the wall.[35]

In the limit of no diffusive resistance (equivalent to ideal plug flow conditions) the continuity equation has a very simple solution, and k_{obs} equals the wall loss rate coefficient k_w, which is obtained by multiplication of κ_w with the reactor's surface-to-volume ratio, $2/r$:

$$k_w = (2/r)\kappa_w \tag{5}$$

In the limit of no surface uptake resistance, k_{obs} equals the diffusion-limited wall loss rate coefficient, k_d. Under fast flow conditions in a cylindrical reactor k_d can be approximated by

$$k_d = \frac{3.66D_g}{r^2} = \frac{3.66D_p}{r^2P} \tag{6}$$

where D_g ($cm^2\ s^{-1}$) is the gas-phase diffusion coefficient defined by Fick's law and D_P (Torr $cm^2\ s^{-1}$) is the pressure-independent diffusion coefficient.[36] Combining eqs 4, 5, and 6 gives

$$\frac{1}{k_{obs}} = \left(\frac{r^2/3.66}{D_p}\right)P + \frac{r/2}{\kappa_w} \tag{7}$$

Thus, a plot of $(1/k_{obs})$ vs pressure should yield a straight line with a slope proportional to $1/D_p$ and an intercept proportional to $1/\kappa_w$. Such a plot is shown in Figure 5 using

the experimental data listed in Table 1. A weighted linear least-squares fit of eq 7 to the data yields a value for $1/\kappa_w = (1.612 \pm 1.264) \times 10^{-4}$ cm^{-1} s and $1/D_p = (14.96 \pm 0.24) \times 10^{-3}$ Torr^{-1} cm^{-2} s; the error bars represent one standard deviation. The corresponding lower, central, and upper values for κ_w are 3480, 6200, and 28 700 cm s^{-1}, and for D_p these values are 65.78, 66.84, and 67.94 Torr cm^2 s^{-1} for H_2SO_4 in N_2/H_2O at 303 K.

Note that the statistical analysis of our results carried out with eq 7 allows a negative intercept in Figure 5 within two standard deviations, which implies a negative wall loss rate coefficient; a zero intercept implies an infinite rate coefficient. Because of the presence of this singularity, a standard nonlinear least-squares fit cannot be directly applied to our data using either Brown's method or the inverse of eq 7, i.e., k_{obs} (in contrast to $1/k_{obs}$) expressed as a function of P and κ_w.

Diffusion Coefficient. The diffusion coefficient value of 66.8 $\pm$ 1.1 Torr cm^2 s^{-1} obtained from the fit of eq 7 is independent of gas-phase water concentrations covered in our experiment—relative humidity (RH) $\leq$3% (H_2O mixing ratio $\leq$0.32). To our knowledge, no measurement of the diffusion coefficient of H_2SO_4 in N_2/H_2O has been reported previously. The measured value is in good agreement with the values estimated by Roedel[37] (H_2SO_4/air at 296 K: $D_p = 60.8$ Torr cm^2 s^{-1}) and by Marti et al.[38] (H_2SO_4 in N_2/H_2O at 303 K and 5% RH: $D_p = 69.2$ Torr cm^2 s^{-1}). Note that a fit of eq 6 to the measured data is shown as the solid line in Figure 4; it implies an infinite value for k_w or $([H_2SO_4]_{ex})_w = 0$ and yields a slightly lower D_p value of about 65 Torr cm^2 s^{-1}.

Marti et al.[38] calculated effective diffusion coefficients for sulfuric acid in N_2/H_2O at relative humidities (RH) ranging from 5% to 20%, taking the formation of gaseous hydrates, $H_2SO_4 \cdot (H_2O)_n$, into consideration. They determined these effective diffusion coefficients following the Enskog−Chapman formalism with sulfuric acid hydrate distributions and diameters calculated according to Kulmala et al.[39] At 303 K and 5% RH they calculated the following hydrate distribution, given in percentages of the total number of gas-phase H_2SO_4 molecules: 65.9% unhydrated H_2SO_4, 31.5% monohydrate, and 3.5% higher hydrates. For 10% RH they calculated a strong increase of hydrate formation (41.4% unhydrated H_2SO_4, 50.0% monohydrate, and 8.6% higher hydrates), i.e., a decrease in the fraction of unhydrated H_2SO_4 of more than one-third, but only a 3% decrease of the effective diffusion coefficient. These theoretical predictions are in agreement with the $[H_2O]$ independence of D_p observed in our experiments. Furthermore, Marti et al. calculated a temperature dependence of less than 2% per 10 K for the effective diffusion coefficient in the range from 298 to 333 K. The low-temperature sensitivity agrees with our observation of no significant dependence of k_{obs} on variations of the average reactor temperature (301−305 K) and on variations of the injector temperature (328−348 K) and the temperature gradients associated with it.

Mass Accommodation Coefficient. The mass accommodation coefficient α is defined as the probability with which a gas molecule colliding with the surface is incorporated into the liquid phase:

$$\alpha = \frac{\text{no. of gas molecules incorporated into the liquid phase}}{\text{no. of gas molecules colliding with the surface}} \quad (8)$$

Equation 8 can also be expressed as a ratio of the total flux into the condensed phase to the total collisional flux to the surface (the flux units being molecules cm^{-2} s^{-1}). In our experiments the total flux of gas-phase sulfuric acid molecules being incorporated into the liquid includes molecules that originated from the liquid upstream in the flow tube. On the other hand, by defining $[H_2SO_4]_{ex}$ as a difference, the corresponding fluxes to the surface are net fluxes that no longer include the evaporation process; the net flux is the total flux minus the flux corresponding to the equilibrium case. Since all the fluxes are directly proportional to the trace gas concentration at the surface, the definition of α given above in terms of a ratio of total fluxes is also valid in terms of the fluxes corresponding to the excess concentration, i.e., the net flux of molecules incorporated into the liquid, J_n, to the net collisional flux to the wall, J_w:

$$\alpha = J_n/J_w \quad (9)$$

J_n is given by eq 3, and the net collisional flux to the wall can be approximated by the following equation from gas kinetic theory:

$$J_w = ([H_2SO_4]_{ex})_w \omega/4 + J_n/2 \quad (10)$$

where ω is the mean thermal molecular velocity, $(8RT/\pi M)^{1/2}$; the $J_n/2$ term arises from the fact that a concentration gradient results in a net velocity component directed toward the surface that needs to be added to ω.[40]

The connection between the accommodation coefficient α and κ_w is obtained by combining eqs 3, 9, and 10:

$$\kappa_w = \frac{\alpha}{1 - \alpha/2}\frac{\omega}{4} \quad (11)$$

For small values of α the expression $\alpha/(1 - \alpha/2)$ can be approximated by α; this amounts to neglecting the $J_n/2$ term in eq 10. Using eq 11 with the best fit κ_w value listed above (6200 cm s^{-1}) yields $\alpha = 0.65$. The lower limit to α, estimated with eq 11 and the best fit $1/\kappa_w$ value minus one standard deviation, is 0.43. The corresponding upper limit value of α is 1.38; the physical upper limit is, of course, unity.

Figure 6 plots the data in Table 1 as k_{obs} versus $1/P$ for

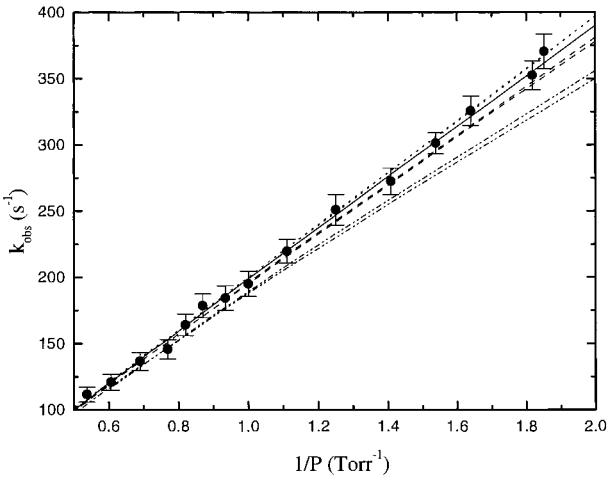

Figure 6. Plot of the observed wall loss rate coefficient as a function of the inverse of the total pressure for pressures less than 2 Torr. The solid line is the linear least-squares fit to the data corresponding to an α value of 0.65 (same as in Figure 5). The pairs of dotted curves in the figure refer to wall loss rates predicted by the method of Brown[32] and the rule of additivity of kinetic resistances for α values of 1.0 (- - -), 0.4 (− − −), and 0.2 (− ·· −). In all cases, the lower curve of each pair is that predicted by the rule additivity of kinetic resistances while the upper curve is obtained by Brown's formulation.

pressures below 2 Torr. The solid line in the figure is the best fit value obtained from Figure 5 (fit of the data to eq 7). The group of dashed lines in Figure 6 are the predicted wall loss rates for values of $\alpha = 1.0$, 0.4, and 0.2 calculated using both the rule of additivity of kinetic resistances (combining eq 7 and eq 11) and calculated from the method of Brown.[32] The dashed lines are computed using the best fit value of $D_p = 66.8$ Torr cm^2 s^{-1}. The calculated k_{obs} values are rather insensitive to values of $\alpha > 0.2$ for the data at pressures above ~2 Torr; this portion of the data contains most of the information related to the diffusive resistance. Clearly, the k_{obs} values for $\alpha = 0.2$ falls outside the experimental error. Figure 6 also shows that the method of Brown,[32] and the rule of additivity of kinetic resistances yields essentially the same results. As a point of comparison, using our value of $D_p = 66.8$ Torr cm^2 s^{-1}, the method of Brown gives $\kappa_w = 3660$ cm s^{-1} ($\alpha = 0.44$), which is within one standard deviation of the value of κ_w obtained from eq 7.

As mentioned before, the observed rate coefficients showed no dependence on the gas-phase concentrations of H_2SO_4 and H_2O. In our experiment, [H_2O] always exceeds the azeotropic H_2O equilibrium vapor pressure at the reactor temperature, and the [H_2O]/[H_2SO_4] ratio always exceeds the azeotropic ratio. This relation holds even when the water vapor source is turned off, which is a consequence of using a heated aqueous sulfuric acid sample as an H_2SO_4 source (the azeotropic [H_2O]/[H_2SO_4] ratio decreases with decreasing temperature[19]). Based on this fact and on the assumption that the condensation process for H_2O molecules (molecular diffusion and mass accommodation) is not any slower than the condensation process for H_2SO_4 molecules, the sulfuric acid wall coating should be in equilibrium with the water partial pressure in the reactor. The composition of the sulfuric acid wall coating in our experiments ranged from 98 to 73 wt %, which corresponds[19] to [H_2O] in the range from 5×10^{12} to 3×10^{16} molecules cm^{-3}, and the mass accommodation coefficient determined before refers to this concentration range. On the other hand, there is no indication that the mass accommodation coefficient for H_2SO_4 on aqueous sulfuric acid would decrease for lower acid concentrations.

Summary

For the mass accommodation coefficient for H_2SO_4 vapor on aqueous sulfuric acid surfaces at 303 K, a best fit value of 0.65 has been determined, with a lower limit of 0.43 (the statistical upper limit is 1.38; the physical upper limit is 1). The mass accommodation process was found to be independent of the liquid surface composition in the range from 73 to 98 wt % H_2SO_4, and there is no indication that it would be less efficient on lower weight percent acid solutions. The gas-phase diffusion coefficient for H_2SO_4 vapor in N_2/H_2O (H_2O mixing ratio ≤ 0.32) was determined to be 66.8 ± 1.1 Torr cm^2 s^{-1}, and to our knowledge this is the first experimental measurement reported; it is consistent with previously calculated values. In determining both the accommodation coefficient and the gas-phase diffusion coefficient, a kinetic model involving the rule of additivity of kinetic resistances was employed. It was shown that for values of $\alpha > \sim 0.2$ the model result is in good agreement with the more rigorous approximate solution to the continuity equation.

The near unity value of the mass accommodation coefficient on aqueous sulfuric acid surfaces implies that ambient H_2SO_4 vapor pressure will be reduced by efficient scavenging on preexisting aqueous aerosols. As a result, atmospheric chemistry models that include aerosol formation and growth processes will predict reduced rates of binary homogeneous water−sulfuric acid nucleation for air masses where sufficient aerosol surface area is available.

Acknowledgment. Financial support for this work was provided by the National Aeronautics and Space Administration's Atmospheric Effects of Aircraft Program under Contract 960501 from the Jet Propulsion Laboratory. We thank Y. Gershenzon for helpful discussions concerning the additivity of kinetic resistances. U. Pöschl thanks the Austrian Science Foundation for financial support, and M. Canagaratna thanks the Dreyfus Environmental Science Postdoctoral Fellowship. J. Jayne thanks S. Clegg for use of his model to calculate water vapor pressures as a function of sulfuric acid composition.

References and Notes

(1) Aerosol Radiative Forcing and Climate Change, National Research Council, National Academy Press, Washington, DC, 1996.
(2) Charlson, R. J.; Schwartz, S. E.; Hales, J. M.; Cess, R. D.; Coakley, Jr., J. A.; Hansen, J. E.; Hofmann, D. J. *Science* **1992**, *255*, 423-430.
(3) Twomey, S. *Atmospheric Aerosols*; Elsevier: New York, 1977.
(4) Abbatt, J. P. D.; Molina, M. J. *Annu. Rev. Energy Environ.* **1993**, *18*, 1−29.
(5) Pandis, S. N.; Russell, L. M.; Seinfeld, J. H. *J. Geophys. Res.* **1994**, *99*, 16945−16957.
(6) Pandis, S. N.; Wexler, A. S.; Seinfeld, J. H. *J. Phys. Chem.* **1995**, *99*, 9646−9659.
(7) Weisenstein, D. K.; Yue, G. K.; Ko, M. K. W.; Sze, N.-D.; Rodriguez, J. M.; Scott, C. J. *J. Geophys. Res.* **1997**, *102*, 13019−13035.
(8) Lin, X.; Chamedies, W. L.; Kiang, C. S.; Stelson, A. W.; Berresheim, H. *J. Geophys. Res.* **1992**, *97*, 18161−18171.
(9) Stockwell, W. R.; Calvert, J. G. *Atmos. Environ.* **1983**, *17*, 2231−2235.
(10) Jayne, J. T.; Pöschl, U.; Chen, Y.-M.; Dai, D.; Molina, L. T.; Worsnop, D. R.; Kolb, C. E.; Molina, M. J. *J. Phys. Chem. A* **1997**, *101*, 10000−10011.
(11) Weber, R. J.; Marti, J. J.; McMurry; Eisle, F. L.; Tanner, D. J.; Jefferson, A. *J. Geophys. Res.* **1997**, *102*, 4375−4385.
(12) Brown, R. C.; Miake-Lye, R. C.; Anderson, M. R.; Kolb, C. E.; Resch, T. J. *J. Geophys. Res.* **1996**, *101*, 22939−22953.
(13) Van Dingenen, R.; Raes, F. *Aerosol Sci. Technol.* **1991**, *15*, 93−106.
(14) Itoh, M. In *Aerosols: Science, Industry, Health and Environment*, Proc. 3rd mt. Conf; Masuda, S., Takahashi, K., Eds.; Pergamon Press: Oxford, UK, 1990; Vol. I, pp 197−200.
(15) Clement, C. F.; Kulmala, M.; Vesala, T. *J. Aerosol Sci.* **1996**, *27*, 869−882.
(16) Nathanson, G. M.; Davidovits, P.; Worsnop, D. R.; Kolb, C. E. *J. Phys. Chem.* **1996**, *100*, 13007−13020.
(17) Jefferson, A.; Eisele, F. L.; Ziemann, P. J.; Weber, R. J.; Marti, J. J.; McMurry *J. Geophys. Res.* **1997**, *102*, 19021−19028.
(18) De Bruyn, W. J.; Shorter, J. A.; Davidovits, P.; Worsnop, D. R.; Zahniser, M. S.; Kolb, C. E. *J. Geophys. Res.* **1994**, *99*, 16927−16932.
(19) *Kirk-Othmer Encyclopedia of Chemical Technology*, 3rd ed.; Wiley: New York, 1983; Vol. 22, p 190.
(20) *Ullmann's Encyclopedia of Industrial Chemistry*; VCH: Weinheim, 1994; Vol. A25, p 635.
(21) Arnold, S. T.; Morris, R. A.; Viggiano, A. A.; Jayne, J. T. *J. Geophys. Res.* **1995**, *100*, 14141.
(22) Viggiano, A. A. Personal Communication Air Force Research Laboratory, Hanscom Air Force Base, MA.
(23) Ayers, G. P.; Gillett, R. W.; Gras, J. L. *Geophys. Res. Lett.* **1980**, *7*, 433.
(24) Giauque, W. F.; Hornung, E. W.; Kunzler, J. E.; Rubin, T. R. *J. Am. Chem. Soc.* **1960**, *82*, 62.
(25) Gmitro, J. I.; Vermeulen, T. *AIChE J.* **1964**, *10*, 740.
(26) Seeley, J. V. Ph.D. Thesis, Massachusetts Institute of Technology, 1994.
(27) Ward-Smith, A. J. *Internal Fluid Flow: The Fluid Dynamics of Flow in Pipes and Ducts*; Clarendon: Oxford, 1980.
(28) Keyser, L. F. *J. Phys. Chem.* **1984**, *88*, 4750.
(29) Taylor, G. *Proc. R. Soc. London, Ser. A* **1953**, *219*, 186.
(30) Murphy, D. M.; Fahey, D. W. *Anal. Chem.* **1987,** *59*, 2753.
(31) Walker, R. E. *Phys. Fluids* **1961**, *4*, 1211.
(32) Brown, R. L. *J. Res. Natl. Bur. Stand.* **1978**, *83*, 1.
(33) Zasypkin, A. Y.; Grigoreva, V. M.; Korchak, V. N.; Gershenzon, Y. M. *Kinet. Catal.* **1997**, *38*, 772−781.

(34) Kolb, C. E.; Worsnop, D. R.; Zahniser, M. S.; Davidovits, P.; Keyser, L. F.; Leu, M.-T.; Molina, M. J.; Hanson, D. R.; Ravishankara, A. R. *Laboratory Studies of Atmospheric Heterogeneous Chemistry*. In *Progress and Problems in Atmospheric Chemistry*; Barker, J. R., Ed.; *Adv. Ser. Phys. Chem*. **1995**, *3*, 771−875.

(35) Frank-Kamenetski, D. A. *Diffusion and Heat Transfer in Chemical Kinetics*; Plenum Press: New York, 1960.

(36) Equation 6 is obtained by solving the continuity equation using the boundary condition $([H_2SO_4]_{ex})_w = 0$ and considering radial diffusion only. Under fast flow conditions axial diffusion can be neglected; the condition given by Murphy and Fahey[30] is $Pe > 10$, where Pe is the Peclet number ($Pe = 2r\nu/D_g$), which was ∼50 here. The axial diffusion correction suggested by Kaufman[41] and Howard[42] affects the flow velocity by less than 1%. Equation 6 follows from neglecting the higher order terms in the series expansion representing the solution to the continuity equation.

(37) Roedel, W. *J Aerosol Sci.* **1979**, *10*, 375.

(38) Marti, J. J.; Jefferson, A.; Cai, X. P.; Richert, C.; MCMurry, P. H.; Eisele, F. *J. Geophys. Res.* **1997**, *102*, 3725.

(39) Kulmala, M.; Mihalis, L.; Laaksonen, A.; Vesala, T. *J. Chem. Phys.* **1991**, *94*, 7411.

(40) Motz, H.; Wise, H. *J. Chem. Phys.* **1960**, *32*, 1893. Jeans, J. *Introduction to the Kinetic Theory of Gases*; Cambridge University Press: New York, 1962. Davison, B. *Proc. Phys. Soc. A* **1951**, *64*, 881.

(41) Kaufman, F. *J. Chem. Phys.* **1984**, *88*, 4904. Kaufman, F. *Science* **1985**, *230*, 393.

(42) Howard, C. J. *J. Phys. Chem.* **1979**, *83*, 3.